DALTON
FULL PAPER

Catalytic action of the iron(II) complexes of 8-methyl-1,4-bis(2-pyridylmethyl)-1,4,8-triazacycloundecane and 1-methyl-5,9-bis(2-pyridylmethyl)-1,5,9-triazacyclododecane

Xiaoping Zhang,[a] Delong Zhang,[a] Daryle H. Busch *[a] and Rudi van Eldik *[b]

[a] *Department of Chemistry, University of Kansas, Lawrence, Kansas, 66045-0046, USA. E-mail: d.busch@eureka.chem.ukans.edu*
[b] *Institute for Inorganic Chemistry, University of Erlangen-Nürnberg, Egerlandstrasse 1, 91058 Erlangen, Germany. E-mail: vaneldik@chemie.uni-erlangen.de*

Received 18th December 1998, Accepted 22nd June 1999

The kinetics and mechanism of the catalatic decomposition of hydrogen peroxide by the iron(II) complexes of the macrocyclic ligands 8-methyl-1,4-bis(2-pyridylmethyl)-1,4,8-triazacycloundecane (L^1) and 1-methyl-5,9-bis(2-pyridylmethyl)-1,5,9-triazacyclododecane (L^2) have been investigated at neutral pH (in phosphate buffer). The oxidation of two equivalents of iron(II) to iron(III) by one equivalent of hydrogen peroxide was observed by spectrophotometric titration. The catalysed decomposition of hydrogen peroxide by iron(III) complex was observed and studied. During the catalytic process a reactive intermediate was scavenged by 2,2′-azinobis(3-ethylbenzothiazoline-6-sulfonate) (ABTS), but not by bromide ion, indicating that the strongly oxidative intermediate is not the hydroxyl radical, and supporting the alternative possibility, a high valent iron–oxo species. Stopped-flow and steady-state kinetic experiments provide further evidence for the detailed mechanism suggested.

Introduction

Oxidation-reduction processes in biological systems often produce the powerful oxidant hydrogen peroxide, which brings the threat of oxidative damage to cellular structure, proteins and metabolites.[1] Certain degenerative and disease states, such as aging[2] and cancer,[3] have been attributed, at least in part, to oxidative damage by H_2O_2. To combat this menace nature evolved the enzyme catalase, which catalyses the decomposition of H_2O_2 to the useful and innocuous products water and dioxygen, eqn. (1). Extensive studies have been devoted to the

$$2\ H_2O_2 \longrightarrow 2\ H_2O + O_2 \qquad (1)$$

understanding of this process.[4–6] The resting state of the catalase enzyme contains an iron(III) heme. For catalase and such related species as peroxidase and cytochrome P450 a molecule of H_2O_2 performs a 2-electron oxidation on the catalytic heme center producing an intermediate species generally referred to as Compound I. Compound I contains an oxoiron(IV) or ferryl species ($^{+\bullet}PFe^{IV}$=O, where P represents porphyrin), with the second oxidation equivalent removing an electron from the heme ring or a component of a neighboring protein side chain, depending on the specific enzyme. The resting state can be recovered by 2-electron reduction of Compound I. The reduction may proceed in two steps, with the radical site generally being reduced first to form Compound II (PFe^{IV}=O), followed by 1-electron reduction of Compound II to restore the iron(III) heme. This simple catalytic cycle is summarized in Scheme 1.

In contrast to the enzymatic process, the mechanism generally accepted for the catalytic decomposition of H_2O_2 by the hydrated ions of iron invokes the free hydroxyl radical as the active oxidant and is commonly described as a "Fenton-like" process[7] (Scheme 2).

$$(PFe^{III}) + H_2O_2 \rightleftharpoons (PFe^{III}(H_2O_2)) \qquad (2)$$

$$(PFe^{III}(H_2O_2)) \longrightarrow (^{+\bullet}PFe^{IV}{=}O) + H_2O \qquad (3)$$

$$(^{+\bullet}PFe^{IV}{=}O) + H_2O_2 \longrightarrow (PFe^{IV}{=}O + HO_2^{\bullet} + H^+) \qquad (4)$$

$$(PFe^{IV}{=}O + HO_2^{\bullet} + H^+) \longrightarrow (PFe^{III}) + H_2O + O_2 \qquad (5)$$

Scheme 1

$$H_2O_2 + (Fe^{III}) \longrightarrow (Fe^{II}) + H^+ + HO_2^{\bullet} \qquad (6)$$

$$(Fe^{II}) + H_2O_2 \longrightarrow (Fe^{III}(OH^-)) + HO^{\bullet} \qquad (7)$$

$$HO^{\bullet} + H_2O_2 \longrightarrow H_2O + HO_2^{\bullet} \qquad (8)$$

$$HO_2^{\bullet} + (Fe^{III}) \longrightarrow O_2 + (Fe^{II}) + H^+ \qquad (9)$$

$$HO_2^{\bullet} + (Fe^{II}) \longrightarrow HO_2^- + (Fe^{III}) \qquad (10)$$

Scheme 2

In seeking to distinguish between these competing models for any given system, primary focus naturally falls on the alternative highly reactive intermediates, the ferryl group or the hydroxyl radical, from Schemes 1 and 2, respectively. If uncontrolled side reactions occur, any related damage is likely to be localized at or near the metal binding site in the case of a ferryl species ($^{+\bullet}PFe^{IV}$=O).[8] To the contrary, damage caused by the hydroxyl radical ($HO^{\bullet}$) might be expected throughout the cellular environment since the biomolecules are sensitive to free-radical damage and common hydroxyl radical scavengers failed to inhibit damage in model systems.[9] The research described here is concerned with the discovery, understanding, and implementation of therapeutic agents for the prevention of H_2O_2 damage in living systems. Owing to the non-selective and random action expected of the hydroxyl radical (Scheme 2) and

† *Supplementary data available*: observed rate constants, rate law deduction. For direct electronic access see http://www.rsc.org/suppdata/dt/1999/2751/, otherwise available from BLDSC (No. SUP 57590, 5 pp.) or the RSC Library. See Instructions for Authors, 1999, Issue 1 (http://www.rsc.org/dalton).

the obvious selective behavior of Compound I in such enzymes as cytochrome P450, catalase, and peroxidase, catalase models are sought that successfully mimic the enzyme mechanism. Our purpose remains to proceed beyond the many porphyrin-based catalase models[10–12] and provide new examples of catalatically efficacious compounds with the long term goal of clarifying the critical parameters that determine the mechanism. Here we seek to build on our earlier success in producing a realistic non-porphyrin model for catalase and peroxidase, dichloro{*meso*-2,12-dimethyl-3,7,11,17-tetraazabicyclo[11.3.1]-heptadeca-1(17),13,15-triene}iron(III) tetrafluoroborate.[13,14] The catalatic process demonstrated by that model complex was tentatively assigned the mechanism of Scheme 1.[14]

From among a family of transition metal complexes with modified triazacycloalkanes that we recently reported,[15,16] significant catalatic activity was found for two iron(II) complexes, those with the pentadentate ligands, 8-methyl-1,4-bis(2-pyridylmethyl)-1,4,8-triazacycloundecane ([11]aneN$_3$MePy$_2$ = L^1) and 1-methyl-5,9-bis(2-pyridylmethyl)-1,5,9-triazacyclododecane ([12]aneN$_3$MePy$_2$ = L^2).[15] Detailed studies on the kinetics and mechanism of the decomposition of hydrogen peroxide catalysed by these complexes are summarized herein. Both pure compounds [Fe^{II}L^{1}Cl][CF$_3$SO$_3$] and [Fe^{II}L^{2}Cl]PF$_6$ contain 6-coordinate and high spin d^6 iron(II).[15,16] In the solid state the sixth co-ordination position is occupied by a chloride ion that is replaced by a water molecule in aqueous solution (written as L^{1}Fe^{II} and L^{2}Fe^{II}).[15,16] Following the guidance of Rush and Koppenol,[17] substrate competition has been used to distinguish between the two possible pathways given by Schemes 1 and 2. Stopped-flow reactions were carried out with and without bromide anion and ABTS (2,2′-azinobis(3-ethylbenzothiazoline-6-sulfonate), Scheme 3), as scavengers. Our results demonstrate the absence of hydroxyl radical, supporting the suggestion that the oxidizing intermediates contain a high valent iron species.

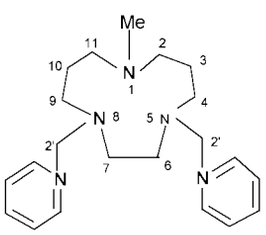

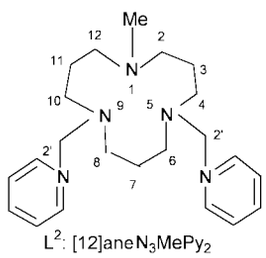

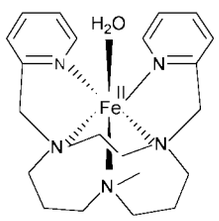

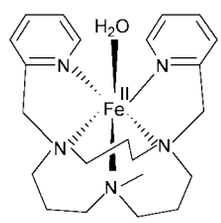

Experimental

Materials

The complexes, [Fe^{II}L^{1}Cl][CF$_3$SO$_3$] and [Fe^{II}L^{2}Cl]PF$_6$, were available from previous studies in this programme.[15,16] Found (Calc.) for [Fe^{II}L^{1}Cl][CF$_3$SO$_3$]: C, 44.39 (44.49); H, 5.00 (5.26); N, 11.99 (11.79)%. Found for [Fe^{II}L^{2}Cl]PF$_6$: C, 43.91 (43.67); H, 5.30 (5.46); N, 11.52 (11.58)%. Deionized, nano-pure water was used for all experiments. 2,2′-Azinobis(3-ethylbenzothiazoline-6-sulfonic acid (ABTS)) diammonium salt was purchased from Sigma. Monobasic potassium phosphate–sodium hydroxide buffer solution (0.10 M, referred to as phosphate buffer in the following text, pH 7.00, Fisher). Background experiment

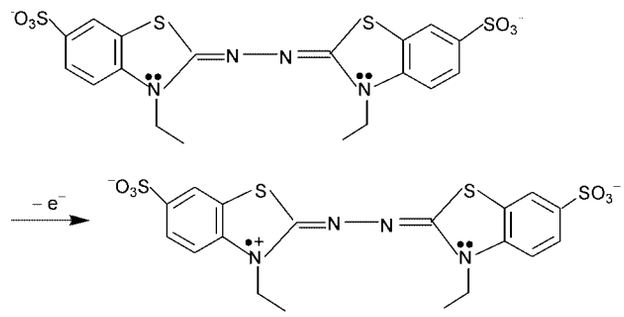

Scheme 3

showed that there is no reaction between complexes and phosphate buffer. The H_2O_2 (35%) was purchased from Aldrich, cerium(IV) sulfate standard solution (0.1000 M) from Fluka. The H_2O_2 solutions were standardized by titration against 0.1000 M Ce^{IV} (stabilized by 1 M H_2SO_4) with Ferroin as indicator.

Instrumentation

The UV-Visible spectra were measured on a Hewlett-Packard 8452A Diode Array Spectrophotometer. Rapid mixing experiments were carried out using a Hi-Tech Model 41 Canterbury Stopped-Flow Spectrophotometer, thermostatted at 25.0 °C. The data were acquired by a Vislen IBM clone computer equipped with an IS-2 rapid kinetic software suite. Calculations of rate constants and their least squares slopes used the same program.

Methods

The first series of kinetic measurements were carried out as follows: one syringe was filled with buffer and H_2O_2 and the other with complex. In the second series of studies ABTS was used as a trap, by adding it to the contents of the first syringe. If solutions of iron(II) complexes are kept for long times in the presence of air oxidation to iron(III) occurs, as indicated by UV-Vis spectral changes. These solutions were therefore prepared freshly for all experiments. The absorbance–time traces were fitted as mentioned above. For experiments in the presence of ABTS the initial rate of the reaction was determined. In this way the complication associated with the further oxidation of $ABTS^{2+}$ can be avoided. The initial rate was calculated by the following method: the initial part of the reaction trace (less than 10% of the complete reaction) was fitted by linear regression. The slope of such a linear plot gives the rate of absorbance change dA/dt. The initial rate, $V_{initial}$, for the formation of $ABTS^{+\bullet}$ can then be calculated by eqn. (11), where ε is the

$$V_{initial} = -\frac{2\,d[H_2O_2]}{dt} = \frac{d[ABTS^{+\bullet}]}{dt} = \frac{dA}{dt}\cdot\frac{1}{\varepsilon b} \qquad (11)$$

absorbance coefficient of $ABTS^{+\bullet}$ at 660 nm (1.2×10^4 M^{-1} cm^{-1})[18] and b is the optical pathlength of the stopped-flow instrument (1 cm). The factor of 2 results from the fact that one mole of hydrogen peroxide oxidizes two moles of ABTS. The temperature was maintained at 25.0 ± 0.2 °C.

Measurement of stoichiometry. For the oxidation of iron(II) to iron(III) by hydrogen peroxide the stoichiometry was determined spectrophotometrically. The absorbance was measured at 320 nm for a series of solutions containing different ratios [H_2O_2]:[L^{1}Fe^{II}]; [L^{1}Fe^{II}] was kept constant at 3.5×10^{-4} M and [H_2O_2] was varied from 0 to 1.4×10^{-3} M. For the catalysed overall reaction the stoichiometry was determined by the following measurement at room temperature and pressure. A 6 mL solution containing 1.96 M H_2O_2 was mixed with 3.0 mg L^{1}Fe^{II}

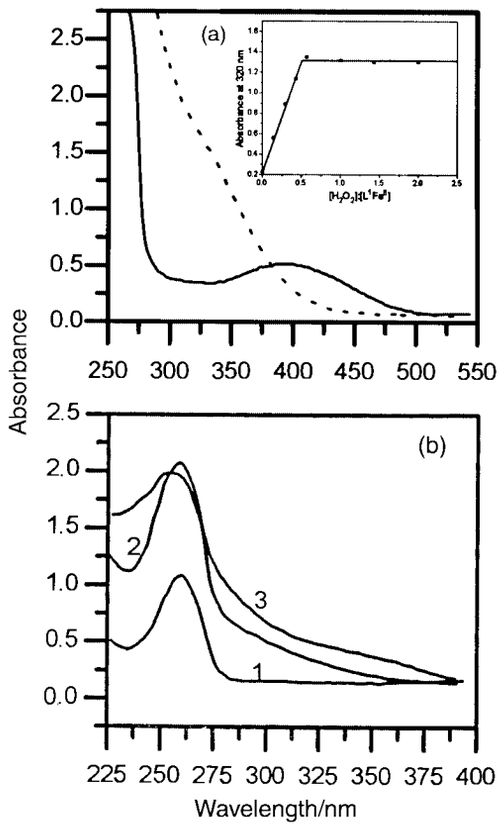

Fig. 1 (a) Absorption spectra of 5.0×10^{-4} M L^1Fe^{II} before (solid line) and after reaction (broken line) with 5.55×10^{-3} M H_2O_2 in 0.05 M phosphate buffer at pH 7.0. Inset: plot of absorbance change *versus* $[H_2O_2]:[L^1Fe^{II}]$ ratio measured at 320 nm using the same buffer solution. Experimental conditions for inset: $[L^1Fe^{II}] = 3.5 \times 10^{-4}$ M; $[H_2O_2] = (1–7) \times 10^{-4}$ M; ionic strength = 0.20 M (phosphate buffer); $T = 25.0 \pm 0.2$ °C. (b) Spectra of L^1Fe^{III} which were obtained by reaction of L^1Fe^{II} with O_2 in air and with H_2O_2 in solution. Key: 1, L^1Fe^{II}; 2, L^1Fe^{III} oxidized by O_2; 3, L^1Fe^{III} oxidized by H_2O_2. Experimental conditions: $[L^1Fe^{II}] = 1 \times 10^{-4}$ M; $[L^1Fe^{III}] = 1 \times 10^{-4}$ M; $[H_2O_2] = 1.5 \times 10^{-3}$ M.

or L^2Fe^{II}. Upon mixing of catalyst with H_2O_2 the generation of O_2 gas was observed. The O_2 gas was collected and its volume determined. The moles of O_2 were calculated from its volume using Boyle's law.[19] The remaining H_2O_2 was titrated cerimetrically and the difference of the H_2O_2 concentrations before and after reaction with catalyst resulted in the moles of H_2O_2 decomposed. From a comparison of the moles of H_2O_2 decomposed with moles of O_2 generated the stoichiometry of the overall catalytic reaction was obtained.

Results and discussion

Stoichiometry of the oxidation reaction

The reaction of L^1Fe^{II} and L^2Fe^{II} with hydrogen peroxide was studied in a phosphate buffer medium at pH 7.0. Typical spectra for L^1Fe^{II} are shown in Fig. 1(a). Before reaction the spectrum (solid line) of L^1Fe^{II} displayed two peaks at 250 ($\varepsilon > 5.6 \times 10^3$) and 395 nm ($\varepsilon = 1.0 \times 10^3$ M^{-1} cm^{-1}). Since iron(II) in these complexes was found to be high spin ($S = 4/2$),[15,16] the spin allowed transition $^5T_{2g} \longrightarrow {}^5E_g$ should occur in the low energy region around 1000 nm.[20] Therefore, these strongly absorbing peaks are assigned to charge transfer (CT) transitions. After reaction with H_2O_2 the spectrum (broken line) was markedly changed and only one broad CT band is observed between 250 and 400 nm with a shoulder at 340 nm; the latter may derive from the $^6A_{1g}(^6S) \longrightarrow {}^4T_{2g}(^4P)$ transition for high spin Fe^{III} ($S = 5/2$).[20] The spectral changes accompanying the oxidation of L^2Fe^{II} to L^2Fe^{III} under the same conditions were very similar to those for L^1Fe^{II}. By increasing $[H_2O_2]/[L^1Fe^{II}]$ the inflection point for the absorbance change occurred at 0.5. The overall stoichiometry of these oxidation reactions is shown in eqn. (12). It was observed that L^1Fe^{II} can be oxidized by air

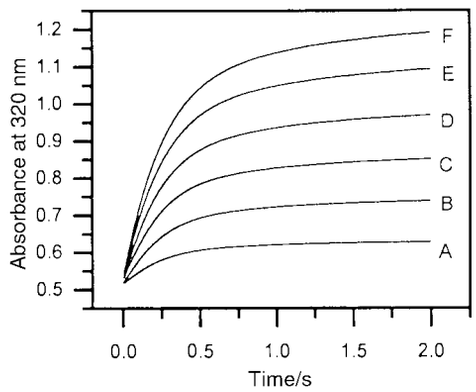

Fig. 2 Typical two-exponential reaction traces recorded in the presence of an excess of L^1Fe^{II} (1.0×10^{-3}M) over H_2O_2. $[H_2O_2] = 15.3$ (trace A), 30.6 (B), 45.9 (C), 61.2 (D), 76.5 (E) and 91.8 μM (F). Experimental conditions: ionic strength = 0.20 M (phosphate buffer); $T = 25.0 \pm 0.2$ °C.

$$2\ L^1Fe^{II} + H_2O_2 + 2\ H^+ \longrightarrow 2\ L^1Fe^{III} + 2\ H_2O \quad (12)$$

to form L^1Fe^{III} (see Fig. 1b). Upon addition of H_2O_2 to the L^1Fe^{III} solution an increase in absorbance between 275 and 400 nm was observed, with a weak band developing at 375 nm (see Fig. 1b). During the reaction of the iron(II) complex with air and H_2O_2 the observed spectral changes are accompanied by a change from colourless to yellow, whereas the addition of H_2O_2 to the iron(III) complex resulted in the development of a faint reddish colour. The latter is ascribed to the formation of $L^1Fe^{III}(H_2O_2)$. We conclude that oxidation of iron(II) to iron(III) occurs no matter whether L^1Fe^{II} or H_2O_2 is in excess. It is a fast reaction process assigned as Path 1.

Stoichiometry of the overall catalatic reaction

In the presence of an excess of H_2O_2 another slow process was observed during which O_2 gas was generated constantly once iron(II) was oxidized to iron(III): 0.13 mmol O_2 was released when 0.26 mmol H_2O_2 reacted in the presence of 6.3×10^{-7} M L^1Fe^{II}. The 0.37 mmol O_2 was released when 0.76 mmol H_2O_2 reacted in the presence of 4.8×10^{-7} M L^2Fe^{II}. These results indicate that the stoichiometry of the overall decomposition reaction is as in eqn. (1). We conclude that the decomposition of H_2O_2 is catalysed by the iron(III) complex assigned as Path 2. The reaction mechanisms will be explored in the following sections.

Kinetics and mechanism of reaction of LFe^{II} with H_2O_2

When the reaction was studied in the presence of an excess of iron(II) complex, LFe^{II}, at a wavelength of 320 nm, typical reaction traces, recorded at different concentrations of hydrogen peroxide (Fig. 2), correspond to a two-exponential equation. The final absorbance increases linearly with increasing $[H_2O_2]$ as shown by the traces A to F in Fig. 2, corresponding to $[H_2O_2]$ of 15.3, 30.6, 45.9, 61.2, 76.5 and 91.8 μM, respectively. This indicates that the reaction sequence consists of two irreversible pseudo-first-order (with X and Y in large excess) reactions (13).[21] The corresponding rate equation (14)

$$A \xrightarrow{(+X)k_a} B \xrightarrow{(+Y)k_b} C \quad (13)$$

$$A_t - A_e = a_1 \exp(-k_{obs1}t) + a_2 \exp(-k_{obs2}t) \quad (14)$$

was derived[21b] where $k_{obs1} = k_a[X]$ and $k_{obs2} = k_b[Y]$. Constants a_1 and a_2 are composed of rate constants and molar absorb-

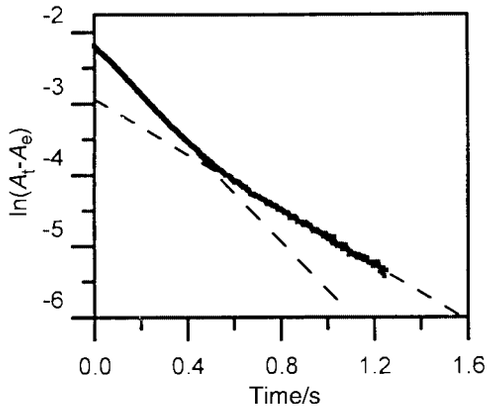

Fig. 3 The logarithmic plot of curve A in Fig. 2 demonstrates the biphasic nature of the reaction. Experimental conditions: see Fig. 2.

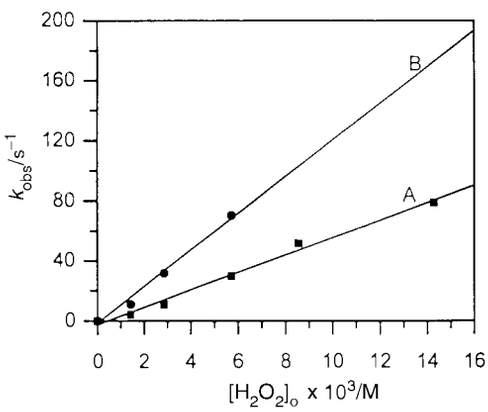

Fig. 4 Linear dependence of observed rate constant k_{obs1} (A) and k_{obs2} (B) for L^2Fe^{II} *versus* initial hydrogen peroxide concentration. Experimental conditions: $[L^2Fe^{II}] = 1.42 \times 10^{-4}$ M; $\lambda = 320$ nm; $T = 25.0$ °C; [phosphate buffer] = 0.05 M (pH 7.0); ionic strength = 0.20 M (phosphate buffer).

ance, A_t and A_e are the absorbances at time t and at the end of the reaction, respectively,[21b] eqns. (15) and (16), where ε_A, ε_B

$$a_1 = \varepsilon_A[A]_o + \frac{\varepsilon_B[A_o]k_a}{k_b - k_a} + \frac{\varepsilon_C[A_o]k_b}{k_a - k_b} \quad (15)$$

$$a_2 = \frac{k_a[A_o](\varepsilon_B - \varepsilon_C)}{k_a - k_b} \quad (16)$$

and ε_C are the absorbance coefficients for A, B and C at a given wavelength. In order to demonstrate that two subsequent reactions are involved, a logarithmic plot was used to show the biphasic nature of the reaction. Fig. 3 is such a plot derived from curve A in Fig. 2.

The observed rate constants, k_{obs1} and k_{obs2}, depend linearly on $[L^2Fe^{II}]$. For L^2Fe^{II} plots of k_{obs1} and k_{obs2} *versus* $[L^2Fe^{II}]$ result in slopes of $(1.4 \pm 0.1) \times 10^4$ and $(5.3 \pm 0.3) \times 10^3$ M^{-1} s^{-1}, respectively.

In the presence of an excess of hydrogen peroxide the absorbance–time traces recorded on the stopped-flow instrument at 320 nm for L^2Fe^{II} were fitted by a two-exponential function at low concentration of $[H_2O_2]$ and by a one-exponential function at high $[H_2O_2]$. It was noticed that the biphasic curve obtained in the presence of an excess of H_2O_2 is similar to Fig. 3. However, at high $[H_2O_2]$ the fast step becomes too fast to be observed and only one exponential function for the slow step was visible. The observed rate constants, k_{obs1} and k_{obs2}, increase linearly with increasing $[H_2O_2]$ as shown in Fig. 4. These plots of k_{obs1} and k_{obs2} *versus* $[H_2O_2]$ result in slopes of $(1.38 \pm 0.05) \times 10^4$ and $(5.7 \pm 0.5) \times 10^3$ M^{-1} s^{-1}, respectively. The values agree closely with the results obtained by varying the concentration of $[L^2Fe^{II}]$. The same experiments were performed for $[L^1Fe^{II}]$. Values for k_{obs1} of $(4.1 \pm 0.4) \times 10^4$ M^{-1} s^{-1} and k_{obs2} of $(1.0 \pm 0.1) \times 10^4$ M^{-1} s^{-1} were obtained.

For the oxidation of the iron(II) to the iron(III) complex (Path 1) the above observed kinetics can be accounted for by reactions (17)–(19). By using the steady-state approximation on the

$$LFe^{II} + H_2O_2 \underset{k_{-1}}{\overset{k_1}{\rightleftharpoons}} LFe^{II}(H_2O_2) \quad (17)$$

$$LFe^{II}(H_2O_2) \underset{k_{-2}}{\overset{k_2}{\rightleftharpoons}} \{LFe^{IV}{=}O\}^{2+} + H_2O \quad (18)$$

$$\{LFe^{IV}{=}O\}^{2+} + LFe^{II} + 2\,H^+ \xrightarrow{k_3} 2\,LFe^{III} + H_2O, \text{ fast} \quad (19)$$

intermediate species, the first irreversible reaction rate law (20) can be derived based on equations (17), (18) and (19). Under the condition that $k_{-1}k_{-2} \ll k_{-1}k_3[LFe^{II}][H^+]^2$, eqn. (20)

$$\frac{d[LFe^{III}]}{dt} = \frac{k_1k_2k_3[LFe^{II}]^2[H_2O_2][H^+]^2}{k_{-1}k_{-2} + k_{-1}k_3[LFe^{II}][H^+]^2} \quad (20)$$

becomes (21). Equation (21) accounts for the observed k_{obs1}

$$\frac{d[LFe^{III}]}{dt} = \frac{k_1k_2}{k_{-1}}[LFe^{II}][H_2O_2] \quad (21)$$

which depends linearly on $[LFe^{II}]$ or $[H_2O_2]$, depending on which one is in excess.

Path 2 represents the catalatic decomposition of H_2O_2 by the iron(III) complex. Since the observed absorbance increase at 320 nm is due to the formation of iron(III), we assume that the second irreversible reaction step is due to the formation of another iron(III) complex, $LFe^{III}(H_2O_2)$. In order to verify this, a solution containing the iron(III) complex (oxidized by air for one day) was mixed with H_2O_2 and the rate constant was determined using the stopped-flow instrument. The absorbance increase was observed at 320 nm and the reaction trace could be fitted by a one-exponential function. The rate constant for L^2Fe^{III} was found to be $(4.4 \pm 0.1) \times 10^3$ M^{-1} s^{-1}, which is close to the value of $(5.3 \pm 0.3) \times 10^3$ M^{-1} s^{-1} obtained from k_{obs2} by fitting a biphasic function to the reaction of L^2Fe^{II} with H_2O_2. The second irreversible reaction is therefore suggested to consist of reactions (22) to (24). We assume that $LFe^{III}(H_2O_2)$ is not

$$LFe^{III} + H_2O_2 \underset{k_{-4}}{\overset{k_4}{\rightleftharpoons}} LFe^{III}(H_2O_2) \quad (22)$$

$$LFe^{III}(H_2O_2) \underset{k_{-5}}{\overset{k_5}{\rightleftharpoons}} \{LFe^{V}{=}O\}^{3+} + H_2O \quad (23)$$

$$\{LFe^{V}{=}O\}^{3+} + H_2O_2 \xrightarrow{k_6} LFe^{III} + O_2 + H_2O \quad (24)$$

stable and undergoes heterolysis and a slow intramolecular electron transfer to generate $\{LFe^{V}{=}O\}^{3+}$, which is immediately reduced by H_2O_2 to the resting iron(III) complex. The rate law (25) can be derived by assuming that $k_{-4} \ll k_4$ and $k_6[H_2O_2] \ll$

$$d[LFe^{III}(H_2O_2)]/dt = k_4[LFe^{II}][H_2O_2] \quad (25)$$

k_{-5}. The obtained eqn. (25) accounts for the linear dependence of k_{obs2} on both $[LFe^{II}]$ or $[H_2O_2]$, depending on which one is in excess. The fact that the second reaction step is observed even under conditions where LFe^{II} is in excess is a result of the difference of only a factor of 2 to 3 between the fast and slow

reactions steps, such that these processes always compete under all experimental conditions.

The intermediate species formed was assumed to be $\{LFe^{IV}=O\}^{2+}$ in reaction (18) and $\{LFe^{V}=O\}^{3+}$ in reaction (23). However, the data presented here could also describe a system in which the intermediate is a hydroxyl radical (Scheme 2). The reaction mechanism for Path 1 would then consist of eqns. (26)–(28). Using steady-state approximations, the rate law (29)

$$LFe^{II} + H_2O_2 \underset{k_{-1}'}{\overset{k_1'}{\rightleftharpoons}} LFe^{II}(H_2O_2) \quad (26)$$

$$LFe^{II}(H_2O_2) \xrightarrow{k_2'} LFe^{III} + OH^- + HO^\bullet \quad (27)$$

$$HO^\bullet + LFe^{II} \xrightarrow{k_3'} LFe^{III} + OH^- \quad (28)$$

$$\frac{d[LFe^{III}]}{dt} = \frac{k_1'k_2'}{k_{-1}' + k_2'}[H_2O_2] \quad (29)$$

which accounts for the first irreversible reaction may be derived from reactions (26) to (28). This rate law indicates that k_{obs1} depends linearly on $[H_2O_2]$, but is independent of $[LFe^{II}]$. Obviously, eqn. (29) does not agree with the experimental findings. In the presence of an excess of H_2O_2, Path 2 takes place *via* eqns. (30)–(35). Using steady-state approximations the rate law

$$LFe^{III} + H_2O_2 \underset{k_{-4}'}{\overset{k_4'}{\rightleftharpoons}} LFe^{III}(H_2O_2) \quad (30)$$

$$LFe^{III}(H_2O_2) \xrightarrow{k_5'} LFe^{II} + H^+ + HO_2^\bullet \quad (31)$$

$$LFe^{II} + H_2O_2 \xrightarrow{k_6'} LFe^{III} + OH^- + HO^\bullet \quad (32)$$

$$H_2O_2 + HO^\bullet \xrightarrow{k_7'} H_2O + HO_2^\bullet \quad (33)$$

$$HO_2^\bullet + LFe^{III} \xrightarrow{k_8'} O_2 + LFe^{II} + H^+ \quad (34)$$

$$HO_2^\bullet + LFe^{II} \xrightarrow{k_9'} HO_2^- + LFe^{III} \quad (35)$$

(36) can be derived $[k_4' \gg (k_{-4}' + k_5')]$. Since the derived rate

$$d[LFe^{III}(H_2O_2)]/dt = k_4'[LFe^{II}][H_2O_2] \quad (36)$$

law for Path 1 does not agree with the experimental data, the reaction mechanism involving an hydroxyl radical is not likely to be operative. In order to verify this conclusion the following experiment was undertaken to distinguish between the two possible mechanisms.

Scavenging oxidizing intermediates with ABTS in the presence and absence of bromide ion

The highly oxidizing intermediate formed in the course of the catalatic process could either be a hydroxyl radical or a higher oxidation state iron species, as discussed above. Rush and Koppenol[8,17,22] developed a method to distinguish between ferryl species and the hydroxyl radical, and their method has been applied in the present study. The free radical scavenger ABTS can be used as a probe for the oxidizing species that are generated under steady-state conditions. The product of reaction of ABTS with $HO^\bullet$, $Br_2^{\bullet -}$ and high valent iron species is the green $ABTS^{+\bullet}$ cation radical, which has an absorption at 660 nm (Scheme 3). As a scavenger in an L^1Fe^{II}/H_2O_2 solution, $ABTS^{+\bullet}$ may be formed either by reaction (37) or (38) in competition with reaction (19) or (24), respectively, or by reaction (39) in competition with reactions (28) and (33). The

$$ABTS + L^1Fe^{IV}=O + 2H^+ \longrightarrow L^1Fe^{III} + ABTS^{+\bullet} + H_2O, \text{ fast} \quad (37)$$

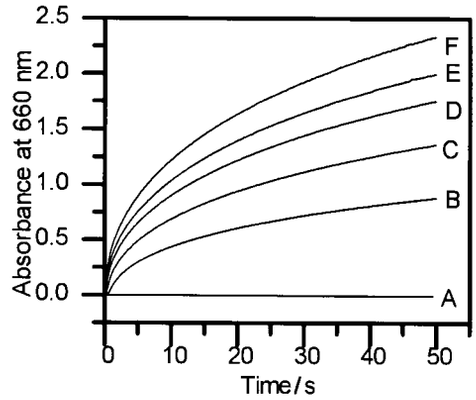

Fig. 5 Reaction traces for the formation of $ABTS^{+\bullet}$ recorded at 660 nm at different concentrations of hydrogen peroxide. Experimental conditions: [phosphate buffer] = 0.05 M; pH 7.0; $[L^1Fe^{II}] = 2.8 \times 10^{-4}$ M, $[ABTS] = 1.0 \times 10^{-3}$ M, $[H_2O_2] = 0$ (trace A), 3.85×10^{-4} (B), 7.65×10^{-4} (C), 11.5×10^{-4} (D), 15.3×10^{-4} (E) and 19.1×10^{-4} M (F); ionic strength = 0.20 M (phosphate buffer); $T = 25.0 \pm 0.2$ °C.

$$2ABTS + L^1Fe^{V}=O + 2H^+ \longrightarrow L^1Fe^{III} + 2ABTS^{+\bullet} + H_2O, \text{ fast} \quad (38)$$

$$ABTS + HO^\bullet \longrightarrow ABTS^{+\bullet} + HO^-, \text{ fast} \quad (39)$$

rate constant for reaction (39) is $k_{39} = 1.2 \times 10^{10}$ M^{-1} s^{-1}.[23] The efficiency of reaction (39) is 58%.[24] In the presence of an excess of bromide ion, hydroxyl radicals will produce the bromine radical anion, $Br_2^{\bullet -}$, eqn. (40), with a reported efficiency of

$$HO^\bullet + 2\,Br^- \longrightarrow HO^- + Br_2^{\bullet -} \quad (40)$$

100%,[8,17,22] and, correspondingly, $Br_2^{\bullet -}$ is totally efficient in its reaction with ABTS, eqn. (41). By comparing the selectivity

$$Br_2^{\bullet -} + ABTS \longrightarrow ABTS^{+\bullet} + 2Br^- \quad (41)$$

and efficiency of the reaction of the intermediate with ABTS in the presence and absence of bromide ion it is possible to distinguish between hydroxyl radical and higher oxidation state iron species, such as $\{L^1Fe^{IV}=O\}^{2+}$ or $\{L^1Fe^{V}=O\}^{3+}$. In control experiments the mixing of ABTS with H_2O_2, or the mixing of ABTS alone with either L^1Fe^{II} or L^2Fe^{II}, did not produce green $ABTS^{+\bullet}$ radicals within the time frame of the experiment. However, the green $ABTS^{+\bullet}$ radical was immediately formed when all three components were mixed. Mixing of the corresponding iron(III) complex with ABTS did not result in the immediate formation of the green $ABTS^{+\bullet}$ radical. The reactions of ABTS with an iron-(II) or -(III) species have, therefore, been negated.

The formation of $ABTS^{+\bullet}$ during the decomposition of hydrogen peroxide in the presence of L^1Fe^{II} or L^2Fe^{II} was monitored at 660 nm. The final concentration, $[ABTS^{+\bullet}]_f$, depended on the initial concentration of H_2O_2 and ABTS, but was independent of the initial concentration of L^1Fe^{II} or L^2Fe^{II}. Fig. 5 shows the formation of $ABTS^{+\bullet}$ as a function of time at different initial hydrogen peroxide concentrations, $[H_2O_2]_o$. The increase in the final absorbance with increasing hydrogen peroxide concentration supports that the LFe^{III} catalyst is recycled during the reaction. Fig. 6 shows the induction period within the first 0.2 s for experiments summarized by Fig. 5. This induction period reflects the time required for the slow build-up of $LFe^{V}=O$, reaction (23). Table 1 shows that the percentage of ABTS oxidized to $ABTS^{+\bullet}$ at 0.2 s is less than 1.04% when reactions (17) to (19) and (22) are completed. We conclude that this is mainly due to the $LFe^{V}=O$ species that is responsible for

Table 1 Estimate for the percentage of [$ABTS^{+\bullet}$] produced within the 0.2 s induction time compared with 100% formation of complex $L^1Fe^{III}(H_2O_2)$. $[L^1Fe^{II}]_o = 2.8 \times 10^{-4}$ M

Trace in Fig. 5	$10^4[H_2O_2]_o$/M	10^3 Initial rate[a]/M s^{-1}	$[L^1Fe^{III}(H_2O_2)]_{0.2s}$[b]/M	$[ABTS^{+\bullet}]_{0.2s}$/M	$[ABTS^{+\bullet}]$[c] (%)
A	0	0	0	0	0
B	3.85	4.4	2.36×10^{-4}	1.67×10^{-7}	0.07
C	7.65	6.2	3.32×10^{-3}	7.50×10^{-7}	0.22
D	11.5	9.4	5.04×10^{-3}	2.33×10^{-6}	0.45
E	15.3	12.6	6.75×10^{-3}	5.67×10^{-6}	0.858
F	19.1	15.6	8.36×10^{-3}	8.83×10^{-6}	1.04

[a] Initial rate = $k_4[H_2O_2]_o[L^1Fe^{III}]_o = 1.1 \times 10^4[H_2O_2]_o[L^1Fe^{II}]_o$. [b] Calculated by initial rate (M s^{-1}) × 0.2 (s). [c] $[ABTS^{+\bullet}]_{0.2s}/[L^1Fe^{III}(H_2O_2)]_{0.2s}$. Experimental conditions: [phosphate buffer] = 0.5 M; $T = 25.0 \pm 0.2$ °C; pH 7.0; ionic strength = 0.20 M (phosphate buffer); $\lambda = 660$ nm.

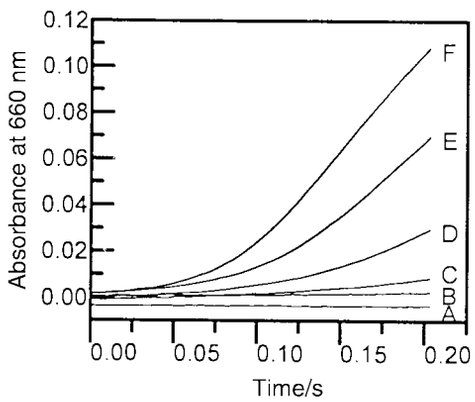

Fig. 6 Kinetic traces showing the induction period for the formation of $ABTS^{+\bullet}$ monitored as a function of time at 660 nm at varying hydrogen peroxide concentrations in 0.05 M phosphate buffer at pH 7.0: $[L^1Fe^{II}] = 2.8 \times 10^{-4}$, $[ABTS] = 1.0 \times 10^{-3}$, $[H_2O_2] = 0$ (trace A), 3.85×10^{-4} (B), 7.65×10^{-4} (C), 11.5×10^{-4} (D), 15.3×10^{-4} (E) and 19.1×10^{-4} M (F). Experimental conditions: ionic strength = 0.20 M (phosphate buffer); $T = 25.0 \pm 0.2$ °C.

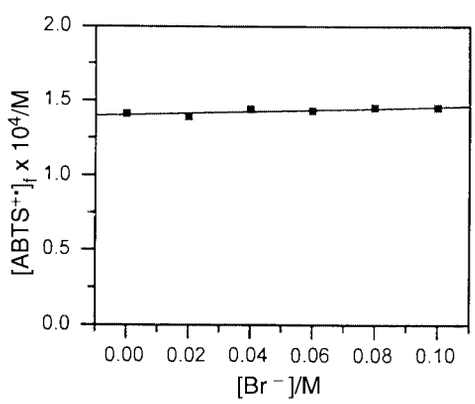

Fig. 7 Dependence of $[ABTS^{+\bullet}]_f$ on the bromide ion added during the scavenging of L^1Fe^{IV}=O by ABTS in 0.05 M phosphate buffer at pH 7.0. $[L^1Fe^{II}] = 2.8 \times 10^{-4}$ M, $[ABTS] = 1.0 \times 10^{-3}$ M, $[H_2O_2] = 1.53 \times 10^{-3}$ M, ionic strength = 0.30 M (phosphate buffer and NaCl or NaBr); $T = 25.0 \pm 0.2$ °C.

the oxidation of ABTS, whereas the intermediate species $LFe^{II}(H_2O_2)$ and $LFe^{III}(H_2O_2)$ do not release hydroxyl radicals since they could not be scavenged by ABTS.

The effect of added bromide ion upon $[ABTS^{+\bullet}]_f$ is shown in Fig. 7. The addition of bromide ion concentrations sufficient to scavenge any hydroxyl radicals (from 0.02 to 0.1 M) causes no increase in $[ABTS^{+\bullet}]_f$ compared to that observed without added bromide ion. This shows that little or no $ABTS^{+\bullet}$ is formed through the intermediacy of $Br_2^{-\bullet}$ or $HO^\bullet$, again suggesting that a hypervalent iron species is the primary oxidant. If the catalatic reaction would take place *via* reaction mechanism (26) to (28) and (30) to (35), the $HO^\bullet$ would have been trapped with 100% efficiency by the bulk Br^- ion to form $Br_2^{-\bullet}$ which consequently reacts with ABTS to produce $ABTS^{+\bullet}$ radical with 100% efficiency. The first point in Fig. 7 represents the $[ABTS^{+\bullet}]_f$ in the absence of Br^-. If the formation of $[ABTS^{+\bullet}]_f$ is due to $HO^\bullet$, the efficiency[23] at this point is as in eqn. (42). In the presence of sufficient Br^- ($[Br^-]/[HO^\bullet] > 13$), the efficiency would be given by eqn. (43). Eqn. (43) would represent other experimental data in Fig. 7 in the presence of Br^-. Combining both (42) and (43), a slope of 1.72 (= 100/58%) for the plot in

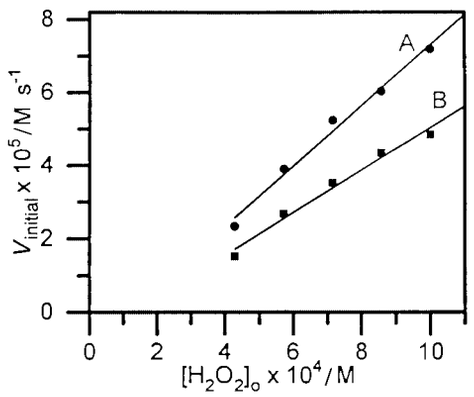

Fig. 8 Dependence of initial rates of formation of $ABTS^{+\bullet}$ ($V_{initial}$/M s^{-1}) on the initial concentration of hydrogen peroxide. Plot A was obtained in the presence of 36 μM $[L^1Fe^{II}]$, B in the presence of 91 μM $[L^2Fe^{II}]$. Experimental conditions: [ABTS] = 0.01 M; [phosphate] = 0.05 M (pH 7); $T = 25.0 \pm 0.2$ °C; ionic strength = 0.20 M (phosphate buffer).

$$d[ABTS^{+\bullet}]_f/d[HO^\bullet] = 58\% \quad (42)$$

$$\frac{d[ABTS^{+\bullet}]_f}{d[HO^\bullet]} = \frac{d[ABTS^{+\bullet}]_f}{d[Br_2^{-\bullet}]} = \frac{d[ABTS^{+\bullet}]_f}{d[Br^-]} = 100\% \quad (43)$$

Fig. 7 would have been obtained. Obviously this is not the case. The slope of the plot in Fig. 7 is almost zero. Therefore we conclude that the catalytic reaction occurs only *via* a higher oxidation state iron species, *i.e.*, reactions (17) to (19) and (22) to (24).

The "initial" rates after induction time for the formation of $ABTS^{+\bullet}$ radical were measured at various hydrogen peroxide concentrations, under the conditions where $[ABTS] > 10[H_2O_2] > 10[LFe^{II}]$. Under these conditions a linear dependence of $V_{initial}$ on $[H_2O_2]$ at $[H_2O_2]$ above 4×10^{-4} M was observed (Fig. 8), giving pseudo first-order rate constants k_{obs3} of 0.0509 (L^1Fe^{II}) and 0.0736 s^{-1} (L^2Fe^{II}) for the formation of $ABTS^{+\bullet}$. Since one equivalent of H_2O_2 produces two equivalents of $ABTS^{+\bullet}$, the H_2O_2 decomposition rate constants 0.0255 (L^1Fe^{II}) and 0.0368 s^{-1} (L^2Fe^{II}) can be obtained according to eqn. (11). These rate constants are assigned to be the turnover rate constant, k_{cat}, for the catalytic cycle of H_2O_2 decomposition. As discussed, the rate determining step is reaction (23), from which we conclude that k_{cat} is mainly the contribution of k_5. Fig. 8 shows that at low concentrations of hydrogen

Table 2 Summary of second-order rate constants for reactions of iron(II) complexes with H_2O_2 at neutral pH

Complex	k_1k_2/k_{-1}/M^{-1} s^{-1}	k_4/M^{-1} s^{-1}	k_5/s^{-1}	k_{cat}/s^{-1}	Ref.
L^1Fe^{II}	$(4.1 \pm 0.4) \times 10^4$	$(1.0 \pm 0.1) \times 10^4$	$(5.09 \pm 0.06) \times 10^{-2}$	$(2.55 \pm 0.03) \times 10^{-2}$	This work
L^2Fe^{II}	$(1.4 \pm 0.4) \times 10^4$	$(5.3 \pm 0.3) \times 10^3$	$(3.68 \pm 0.08) \times 10^{-2}$	$(3.68 \pm 0.04) \times 10^{-2}$	This work
Fe^{II}(DTPA)	1.37×10^3				24
Fe^{II}(HEDTA)	4.2×10^4				17
Fe^{II}(NTA)	3.0×10^4				17
Fe^{II}(EDDA)	7.8×10^4				17

H_5DTPA = Carboxymethyliminobis(ethylenenitrilo)tetraacetic acid, HEDTA = *N'*-(2-hydroxyethyl)ethylenediamine-*N*,*N*,*N'*-triacetate, H_3NTA = nitrilotriacetic acid, and H_2EDDA = ethylenediiminodiacetic acid.

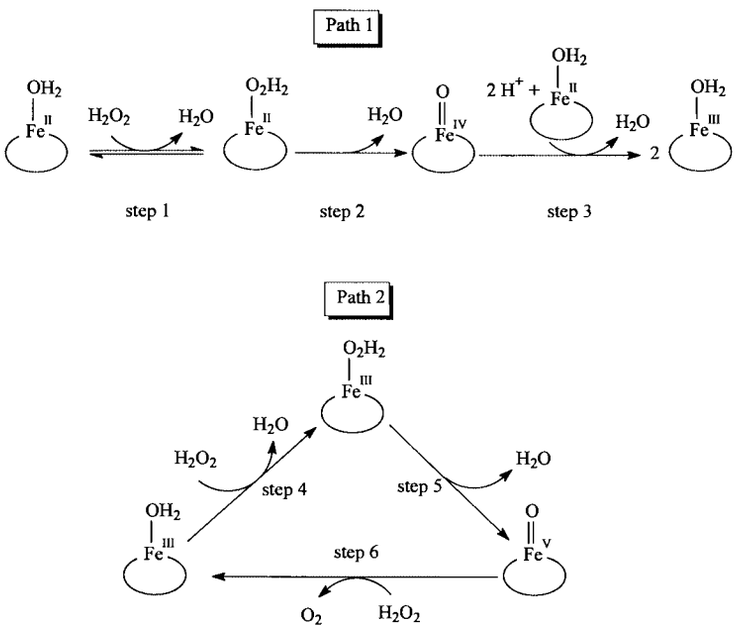

Scheme 4

peroxide the formation of $ABTS^{+\bullet}$ radical does not occur. This is consistent with our previous conclusion that only the intermediate $\{LFe^{V}=O\}^{3+}$ is active toward the oxidation of ABTS and the intermediates $LFe^{II}(H_2O_2)$ and $LFe^{III}(H_2O_2)$ are inactive toward the same reaction, *i.e.* the latter do not release hydroxyl radicals.

The rate constants k_1k_2/k_{-1}, k_4 and k_5 are summarized in Table 2 along with literature values of second-order reaction rate constant for the reaction of other iron(II) complexes with hydrogen peroxide. Studies on the reactions of Fe^{II}(DTPA),[24] Fe^{II}(HEPTA),[17] Fe^{II}(NTA),[17] and Fe^{II}(EDDA)[17] with H_2O_2 all support higher oxidation state iron intermediates in their reactions with H_2O_2 instead of the hydroxyl radical. Our results for the reactions of two macrocyclic complexes with H_2O_2 extend the realm of such intermediates to iron catalysts based on macrocyclic ligands.

Overall reaction mechanism

The overall reaction mechanisms are summarized in Scheme 4. Path 1 is the oxidation of LFe^{II} to LFe^{III}. The rate limiting step is the substitution of co-ordinated water by H_2O_2 to form LFe^{II}-(H_2O_2) (step 1); this is not stable and undergoes heterolysis and an intramolecular electron transfer reaction to produce an intermediate $\{LFe^{IV}=O\}^{2+}$ (step 2). The latter is reduced by another molecule of LFe^{II} to yield two equivalents of LFe^{III} (step 3). Path 2 is the catalytic decomposition of H_2O_2 by LFe^{III}. The first step is the fast substitution of co-ordination water by H_2O_2 to produce $LFe^{III}(H_2O_2)$ (step 4). This undergoes heterolysis and an intramolecular electron transfer reaction to produce $\{LFe^{V}=O\}^{3+}$ (step 5) which is subsequently reduced by H_2O_2 to generate O_2 (step 6). Direct evidence for the nature of the suggested intermediates remains to be explored.

Finally, this study demonstrates that the investigated macrocyclic iron(II/III) complexes are active as mimics for catalase, proceeding through a high valent iron intermediate to catalyse the decomposition of hydrogen peroxide. The high valent iron intermediate causes less damage to the ligand and other possible substrates than freely diffusing hydroxyl radicals.

Acknowledgements

We gratefully acknowledge the financial support of the Monsanto Company.

References

1 J. A. Cowan, *Inorganic Biochemistry*, Wiley VCH, Inc., New York, 1997, p. 319.
2 P. L. Mote, J. M. Crizzle, R. L. Walford and S. R. Spindler, *J. Gerontol.*, 1991, **46**, 95.
3 I. Durak, A. C. U. Isik, O. Canbolat, O. Akyol and M. Kavutcu, *Free Radical Biol. Med.*, 1993, **15** , 681.
4 M. R. N. Murthy, T. J. Reid, A. Sicignano, N. N. Tanaka and M. G. Rossmann, *J. Mol. Biol.*, 1981, **152**, 465; I. Fita and G. Rossman, *J. Mol. Biol.*, 1985, **185**, 21.
5 W. R. Melik-Adamyan, V. V. Barynin, A. A. Vagin, V. V. Borisvo, B. K. Vainshtein, I. Fita, R. N. Murthy and M. G. Rossman, *J. Mol. Biol.*, 1986, **188**, 63.
6 B. K. Vainshtein, W. R. Melik-Adamyan, V. V. Barynin, A. A. Vagin, A. I. Grebenko, V. V. Borisvo, K. S. Bartels, I. Fita and M. S. Rossman, *J. Mol. Biol.*, 1986, **188**, 49; S. Otsuka and T. Yamanaka, *Metalloproteins-Chemical Proteins and Biological Effects*, Kodansha LTD, Tokyo, 1988, p. 227.
7 H. J. H. Fenton, *J. Chem. Soc.*, 1894, **65**, 899.
8 J. D. Rush and W. H. Koppenol, *J. Inorg. Biochem.*, 1987, **29**, 199; *J. Biol. Chem.*, 1986, **261**, 6730.

9 A. Samuni, J. Aronovitch, D. Grodinger, M. Chevion and G. Czapski, *Eur. J. Biochem.*, 1983, **137**, 119; C. C. Winterbourn and H. C. Sutton, in *Oxygen Radicals in Chemistry*, eds. W. Bors, N. Saran and D. Tait, De Gruyter, New York, 1984, pp. 185–191.
10 J. R. L. Smith, P. N. Balasubramania and T. C. Bruice, *J. Am. Chem. Soc.*, 1988, **110**, 7411; A. Robert, B. Loock, M. Momenteau and B. Meunier, *Inorg. Chem.*, 1991, **30**, 706.
11 J. H. Dawson, *Science*, 1988, **240**, 433.
12 K. Murata, R. Panicucci, E. Gopinath and T. C. Bruice, *J. Am. Chem. Soc.*, 1990, **112**, 6072.
13 A. C. Melnyk, N. K. Kildahl, A. R. Rendina and D. H. Busch, *J. Am. Chem. Soc.*, 1979, **101** , 3232.
14 C. J. Cairns, R. A. Heckman, A. C. Melnyk, W. M. Davis and D. H. Busch, *J. Chem. Soc.*, *Dalton Trans.*, 1987, 2505.
15 D. L. Zhang, Ph.D. Thesis, University of Kansas, Lawrence, Kansas, 1994.
16 D. L. Zhang and D. H. Busch, *Inorg. Chem.*, 1994, **33**, 5138.
17 J. D. Rush and W. H. Koppenol, *J. Am. Chem. Soc.*, 1988, **110**, 4957.
18 S. Huenig, H. Balli, H. Conrad, A. Schott and L. Justus, *Anal. Chem.*, 1964, **676**, 36.
19 D. D. Ebbing and M. S. Wrighton, *General Chemistry*, Houghton Mifflin Company, Boston, 1984, p. 91.
20 C. J. Ballhausen, *Introduction to Ligand Field Theory*, McGraw-Hill, New York, 1962, pp. 251–255.
21 (*a*) *Instruction Manual IS-2 Rapid Kinetics Software*, Hi-Tech Scientific Limited, Salisbury, 1993, p. 29; (*b*) R. G. Wilkins, *Kinetics and Mechanism of Reactions of Transition Metal Complexes*, 2nd thoroughly revised edition, VCH, New York, p. 19.
22 J. D. Rush and W. H. Koppenol, *J. Biol. Chem.*, 1986, **261**, 6730.
23 K. P. Kundu and N. Matsuru, *Int. J. Radiat. Phys. Chem.*, 1971, **3**, 1.
24 S. Rahhal and H. W. Richter, *J. Am. Chem. Soc.*, 1988, **110**, 3126.

Paper 8/09866B